Assessment of subfilter-scale turbulence-radiation interaction in non-luminous pool fires

Fatiha Nmira, Li Ma, Jean-Louis Consalvi

Version of Record: https://www.sciencedirect.com/science/article/pii/S1540748920303631
Manuscript_95fa9f2c0fd5caf6c721cd12c32735d3

Assessment of subfilter-scale turbulence-radiation interaction in large-scale, non-luminous pool fires

Fatiha Nmira[1], Li Ma[1,2], Jean-Louis Consalvi[2,†]

[1] Direction R&D EDF, 6 quai Watier, 78400 Chatou, France.

[2]Aix-Marseille Université, CNRS, IUSTI UMR 7343, 5 rue E. Fermi, 13013 Marseille, France.

Abstract:

The objective of this work is to investigate the effects of Turbulence-Radiation Interaction (TRI) in Large Eddy Simulation (LES) of ethanol pool fires ranging from medium to large sizes. LES of three pool fires are performed using a steady laminar flamelet (SLF)/presumed Filtered Density Function (FDF) combustion model and the Rank Correlated Full Spectrum k-distribution (RC FSK) for spectral gas radiation. Subfilter-scale (SGS) absorption TRI is neglected whereas the filtered emission term is modelled from the presumed FDF approach. The baseline case is the 0.5m diameter pool fire investigated experimentally by Fischer et al. (Combust. Flame 70 (1987) 291-306). The two other synthetic pool fires were generated by scaling the pool diameter by factors of 2 and 4 while maintaining the fuel mass burning rate per unit area unchanged. Predictions in terms of temperature, mole fractions of radiating species, flame puffing frequency and radiant fraction are in good agreement with the available experimental data. Model results show that TRI accounts for at least 80% of the radiative loss. For LES that resolves more than 80% of the temperature variance, the SFS TRI contributes for a non-negligible part to radiative loss and its contribution increases significantly with the pool size. Neglecting it affects significantly the predictions of the fire plume structure and radiative heat flux even for medium-scale pool fires.

Key Words: Ethanol Pool Fire, Large Eddy Simulation, Turbulence-Radiation Interaction, Subfilter-Scale TRI.

1. Introduction

TRI refers to the contribution of turbulent fluctuations in temperature and composition to the mean radiation emission and absorption terms. Their importance for the prediction of the radiative structure of pool fires was evidenced and quantified in past studies (see Refs. [1]-[10]) for example). Snegirev [3] provided RANS simulations of propane pool fires with a Monte Carlo method. Emission TRI was modelled by expanding the emission term into a Taylor series and truncated with two constants adjusted to match the experiments. This approach was recently revisited by fitting the unclosed high-order terms from LES in non-luminous pool fire configurations [4]. Krishnamoorthy et al. [5] and Consalvi et al. [6] used decoupled radiative transfer calculations to investigate different spectral models in pool fires. Concerning the modelling of emission TRI Krishnamoorthy et al. [5] applied the TRI model of Snegirev whereas a presumed PDF approach was considered in Ref. [6]. RANS simulations of pool fires using the SLF/presumed PDF model were also reported in Refs. [7],[8]. The radiative transfer equation (RTE) was solved with the Finite Volume Method coupled to the Full-Spectrum Correlated-k model. The emission TRI was modelled directly from the presumed PDF. The radiant fraction of medium-scale methane fire plume was found increase by 89% when TRI is taken into account [7]. This strong enhancement in radiative loss owing to TRI in non-sooting flame was also observed in Refs. [9],[10], where the resolved-scale turbulence-radiation interaction (TRI) effects in lab-scale ethanol pool fires was investigated.

LES has become the standard for fire modelling over the last twenty years [11]-[17]. In LES, a part of turbulent fluctuations and their contribution to TRI are directly resolved whereas the contributions of SFS TRI requires to be modelled. Modelling works on turbulent jet diffusion

flames showed that the SFS absorption TRI can be neglected even for large-scale flames [18],[19]. FDF approaches consider all the correlations affecting the SFS emission TRI and provide an accurate modelling of this term. The contribution of SFS emission TRI was found to be significant in both lab- and large-scale jet diffusion flames [18]-[20]. As to date most of LES of pool fires ignored SFS TRI [9]-[12],[15],[16]. Noticeable exceptions are the works reported in Refs. [14],[17],[21] where SFS emission TRI was modelled in a simplified manner by extending the Snegirev's model to LES.

The objectives of the article is to quantify the contributions of resolved and SFS TRI to radiative loss in ethanol pool fires ranging from medium to large sizes and the effects of SFS TRI on the prediction of the fire plume structure. To the authors' best knowledge, such an evaluation was not reported in the literature. The article is organized as follows. It begins with the presentation of the numerical model. Next, numerical results are compared with the available experimental data and TRI effects are discussed. Finally, the conclusions drawn from the present study are summarized.

2. Numerical model

2.1. Governing equations

The Favre filtered Navier-Stokes equations, supplemented with transport equations for the filtered enthalpy, $\tilde{h}$, mixture fraction, $\tilde{Z}$, and second moment of the mixture fraction, $\widetilde{Z^2}$, are solved by using the second-order iterative variable-density solver developed by Ma et al. [22] and implemented in the finite volume code *Code_Saturne* v5.0.9 [23]. The SFS momentum stresses and scalar fluxes are modelled using the dynamic Smagorinsky and eddy diffusivity models [24], respectively.

The combustion is modelled using an enthalpy defect SLF model which parametrizes the local thermochemical state by the mixture fraction, Z, the scalar dissipation rate, χ, and the enthalpy defect, $X_R = h - h_{ad}$, where h_{ad} is the adiabatic enthalpy [25]. The flamelet library was generated using the mechanism of ethanol oxidation developed by Saxena and Williams [26]. The filtered thermochemical quantities are then obtained by employing a presumed joint FDF of Z, χ and X_R. Z, χ and X_R are assumed to be statistically independent and the marginal FDFs are modelled by a β distribution for Z and δ-distributions for χ and X_R. The β–distribution cannot describe the bimodal behavior observed in buoyant flames owing to the puffing process and, as a result, is not relevant for RANS [13]. However, it is expected to be more appropriate for LES since a significant part of the large-scale induced intermittency is directly resolved [13]. The Favre-filtered form of the thermochemical look-up table can eventually be expressed in terms of $\tilde{Z}, \widetilde{Z''^2}, \tilde{\chi}, \tilde{X}_R$ [27]. Here $\widetilde{Z''^2}$ represents the subfilter variance of Z which needs to be modelled. In this work, we consider a transport equation for $\widetilde{Z^2}$ (Second Moment Transport Equation, STE) with the subfilter variance being then calculated from its definition, $\widetilde{Z''^2} = \widetilde{Z^2} - \tilde{Z}^2$. This approach is preferred to a direct solution of the variance transport equation since this latter introduces a production term, which is susceptible to large numerical errors [28]. The remaining modelling step for STE concerns the filtered scalar dissipation rate, $\tilde{\chi}$. This term is splitted into resolved, $\tilde{\chi}_{ReS}$, and subfilter, $\tilde{\chi}_{SFS}$, components [28]. $\tilde{\chi}_{SFS}$ is modelled as $\tilde{\chi}_{SFS} = C_Z \frac{(\tilde{D}+D_T)}{\Delta^2} \widetilde{Z''^2}$ where $\tilde{D}$ and D_T are the molecular and turbulent diffusivity, respectively. C_Z is obtained by using the dynamic procedure proposed in Ref. [29].

2.2. Radiation model

2.2.1. Gas radiative property model

The spectral coverage range in terms of wavenumber, η, is 0-25000 cm^{-1} and H_2O and CO_2 are considered as the only radiating species. Soot radiation is disregarded since Fischer and Grosshandler found its contribution negligible [30]. Our simulations showed that the CO contribution can also be neglected. The RC FSK method is used as gas radiative property model [31]. As in the classical FSK [32], the FS cumulative k-g distribution function, is defined as $g(k,\phi,T_p) = \int_0^\infty H[k-\kappa_\eta(\phi)]\, I_{b\eta}(T_p)d\eta / I_b(T_P)$, where H is the Heaviside function, κ_η is the spectral absorption coefficient, $\phi = \{x_{CO2}, x_{H2O}, T\}$ is an array of thermodynamic variables affecting κ_η. x_{CO2} and x_{H2O} represent the mole fractions of CO_2 and H_2O, respectively. $I_{b\eta}$ and I_b are the spectral and total blackbody intensities at the blackbody temperature, T_p, respectively. The main advantage of the RC FSK is that it does not require any specification of a reference state [31]. Mixed FS k-g distributions (for mixtures of H_2O and CO_2) are constructed from HITEMP 2010 [33] by using the procedure proposed by Modest and Riazzi [32]. The FSK radiative transfer equation can be written as:

$$\frac{dI_{g_0}}{ds} = -k^*(g_0)I_{g_0} + k^*(g_0)a(g_0)I_b(T) \quad (1)$$

where g_0 corresponds in the present study to a quadrature-point of a 10-point Gauss-Legendre quadrature scheme and I_{g_0} is the radiative intensity at this quadrature point [31]. The RC FSK scheme determines the absorption coefficient by solving $g(k^*,\phi,T_p) = g_0$ whereas the stretching function is computed as $a = \partial g[k(g_0,\phi,T_p),\phi,T]/\partial g_0$ [31]. The total radiative intensity, I, and the total incident radiation, G, are computed as $I = \int_0^1 I_{g_0}\, dg_0$ and $G = \int_{4\pi} I d\Omega$, respectively. The divergence of the radiative flux is then calculated from the following equation:

$$\nabla \cdot \dot{q}_R'' = \underbrace{\int_0^1 4\pi\, k^* a I_b dg_0}_{\dot{Q}_{em}'''} - \underbrace{\int_0^1 k^* G\, dg_0}_{\dot{Q}_{abs}'''} \tag{2}$$

Predictions were found insensitive to the choice of T_p. In the present simulations, T_p was set equal to 1500K.

2.2.2. Filtered RTE

The filtered RTE and divergence of the radiative flux are obtained by applying the filtering operation to Eqs. 1 and 2:

$$\frac{d\overline{I_{g_0}}}{ds} = -\overline{k^* I_{g_0}} + \overline{k^* a I_b} \tag{3}$$

$$\overline{\nabla \cdot \dot{q}_R''} = \int_0^1 4\pi\, \overline{k^* a I_b} dg_0 - \int_0^1 \overline{k^* G}\, dg_0 \tag{4}$$

SFS absorption TRI is neglected, leading to $\overline{k^* I_{g_0}} \approx \overline{k^*}\,\overline{I_{g_0}}$ and $\overline{k^* G} \approx \overline{k^*}\,\overline{G}$. Gupta et al. [18] showed that this approximation is valid in turbulent flames when more than 80% of turbulent fluctuations are resolved as it is the case in the present study (see section 3.3). The filtered absorption coefficient and emission terms are closed by using the presumed FDF approach:

$$\overline{k^*} = \bar{\rho} \int \frac{(k^*)^{fl}(Z, \tilde{\chi}, \widetilde{X_R})}{\rho^{fl}(Z, \tilde{\chi}, \widetilde{X_R})} \beta\left(Z; \tilde{Z}, \widetilde{Z''^2}\right) dZ \tag{5}$$

$$\overline{k^* a I_b} = \bar{\rho} \int \frac{(k^* a I_b)^{fl}(Z, \tilde{\chi}, \widetilde{X_R})}{\rho^{fl}(Z, \tilde{\chi}, \widetilde{X_R})} \beta\left(Z; \tilde{Z}, \widetilde{Z''^2}\right) dZ \tag{6}$$

where the superscript fl refers to the flamelet library.

The Filtered RTE is solved by using the Discrete Ordinates Method with a S8 quadrature scheme [34]. This angular resolution was selected based on Ref. [35], which demonstrated

that a S4 quadrature is sufficient within the flame, where radiation is isotropic, whereas a finer quadrature is required to predict accurately flux outside the fire.

2.3. Analysis of TRI

TRI represents the contributions of the turbulent fluctuations to the mean absorption and emission terms. In the following, $\langle\phi\rangle$ and ϕ' will denote the time-averaged value and the fluctuation of ϕ, respectively.

In LES, the contribution of turbulent fluctuations in temperature and mole fractions of the radiating species to TRI is decomposed into resolved-scale fluctuations, ReS TRI, and subfilter-scale fluctuations, SFS TRI. These latter requires modelling. Different closures for the filtered absorption and emission terms were investigated in order to quantify the effects of ReS TRI and SFS TRI on the radiative loss and are summarized in Table 1. The filtered absorption and emission terms were evaluated from: i) $\langle\tilde{T}\rangle$, $\langle\tilde{x}_{CO2}\rangle$ and $\langle\tilde{x}_{H2O}\rangle$ by ignoring all the fluctuations (No TRI), ii) $\tilde{T}$, $\tilde{x}_{CO2}$ and $\tilde{x}_{H2O}$ by considering only the resolved fluctuations (ReS TRI) and then ignoring the SFS TRI, and iii) Eqs. 5 and 6 based on presumed FDF that allows taking into account both ReS and SFS fluctuations (Full TRI). $\overline{k^*}$ and $\overline{k^* a I_b}$ are included in the 4D look-up table parametrized by $\tilde{Z}, \widetilde{Z''^2}, \tilde{\chi}, \tilde{X}_R$. Consequently, the increase in CPU time is marginal as compared to the ReS TRI case.

Radiation is solved in coupled manner for both Res TRI and Full TRI cases and in decoupled manner for the No TRI case by using $\langle\tilde{T}\rangle$, $\langle\tilde{x}_{CO2}\rangle$ and $\langle\tilde{x}_{H2O}\rangle$ obtained from the Full TRI simulations.

Table 1. Different TRI closures for filtered absorption and emission terms.

Case	Absorption	Emission
No TRI	$k^*(\langle\tilde{\phi}\rangle)\langle\bar{G}\rangle$	$k^*(\langle\tilde{\phi}\rangle)a(\langle\tilde{\phi}\rangle,\langle\tilde{T}\rangle)I_b(\langle\tilde{T}\rangle)$

ReS TRI	$k^*(\tilde{\phi})\bar{G}$	$k^*(\tilde{\phi})a(\tilde{\phi},\tilde{T})I_b(\tilde{T})$
Full TRI	$\overline{k^*\bar{G}}$	$\overline{k^*aI_b}$

3. Results and discussions

3.1. Ethanol pool fires

The baseline configuration is the 0.5m diameter ethanol pool fire investigated experimentally by Fischer et al. [1]. This pool fire is characterized by a heat release rate (HRR, $\dot{Q}$) of 72.8 kW. According to Fisher et al. [1], the measured fire plume is over-ventilated. Consequently, the configuration was simplified by considering a 3×3×3m^3 domain with free boundary condition on the domain sides. It was checked that the dimension of the domain does not affect the flow and heat transfer. Consistently with the experiments, the fuel pan is located on a solid support at 1m above the floor and surrounded by a steel collar with an outside diameter of 1.1m and a burner rim height of 10mm is considered. This latter point was found to play an important role on the pool dynamics. A structured mesh with 3.75×10^6 cells is considered. The mesh is refined with cell size of 5 mm×5 mm×5 mm in a box of 0.6m×0.6m×0.6m located above the fuel pan. The cell size is progressively stretched toward the boundaries. The simulations relative to this flame will be referred to as F1D hereafter.

To analyse the effects of the flame optical thickness, two synthetic pool fires are simulated by scaling up the pool diameter by 2 and 4 while maintaining the same fuel mass burning rate per unit area. A simple geometric scaling of the computational mesh is considered for all flames. The simulations relative to these flames are referred to as F2D and F4D, respectively. The flame configurations are summarized in Table 2. The fourth column provides the plume resolution index (PRI), defined as the ratio between the plume characteristic length scale, $D^* = \left(\dot{Q}/\rho_\infty c_p T_\infty \sqrt{g}\right)^{2/5}$, and the grid size, Δ. ρ_∞, c_p, and T_∞ represent the density, heat capacity and temperature of ambient air, respectively, whereas g denotes the gravity. The PRI

characterizes the quality of the resolution with higher values corresponding to a better resolution of the fire dynamics [15],[16]. The PRI reported in Table 2 are consistent with the highest resolution reported in the literature for similar simulations.

Concerning the boundary conditions, typical outflow and entrainment boundary conditions are used for open boundaries at the outlet and sides, respectively. The evaporation process of ethanol is disregarded and the pool surface is treated as a gaseous fuel inlet boundary condition. The fuel mass burning rate is maintained constant to provide the specified HRR and both convective and diffusive mass and energy fluxes are accounted for. This simplified treatment does not consider the TRI effects on the radiative feedback to the pool surface that could affect the evaporation rate and, in turn, combustion and radiation processes, including TRI.

Throughout all simulations, time step is set to 5×10^{-4} s, and simulations run for 30 s. The time-averaged mean and rms values were collected at each time step from 6 s. The first 6 s of simulation were used to establish a statistically stationary flow.

Table 2. Flame configurations. χ_{em} and $\dot{Q}_{abs}/\dot{Q}_{em}$ are computed with the Full TRI model.

Flames	D (m)	HRR $\dot{Q}$ (kW)	$\frac{D^*}{\Delta}$ (-)	$\frac{\dot{Q}_{em}}{\dot{Q}}$ (-)	$\frac{\dot{Q}_{abs}}{\dot{Q}_{em}}$ (-)
F1D	0.50	72.8	66.8	0.47	0.57
F2D	1.00	291.2	58.0	0.62	0.65
F4D	2.00	1164.8	50.0	0.82	0.70

3.2. Comparison with available experimental data

This section presents the comparison between LES and the experimental data of Fisher et al. [1]. Figures 1 and 2 show that a satisfactory agreement is observed for the radial profiles of mean temperature and mole fractions of CO_2, H_2O and CO. Radial profiles of temperature fluctuations and the corresponding discussion are provided in Supplemental data (Fig. S1).

The predicted puffing frequency of 1.67Hz compares also reasonably well with the measured one of 1.96Hz [1].

The radiant fraction is defined as $\chi_R = \left(\dot{Q}_{em} - \dot{Q}_{abs}\right)/\dot{Q}$ where $\dot{Q}_{em} = \int_V \dot{Q}'''_{em} dV$ and $\dot{Q}_{abs} = \int_V \dot{Q}'''_{abs} dV$ are the total emission and total absorption, respectively, and V is the volume of the computational domain. For F1D, the computed value of 0.202 obtained with the Full TRI model compares well with the measured one of 0.19 [1]. The computed value was obtained over the entire domain and a closer prediction of 0.185 is computed if only the first 0.75 m of the flame is considered as in the experiments [1].

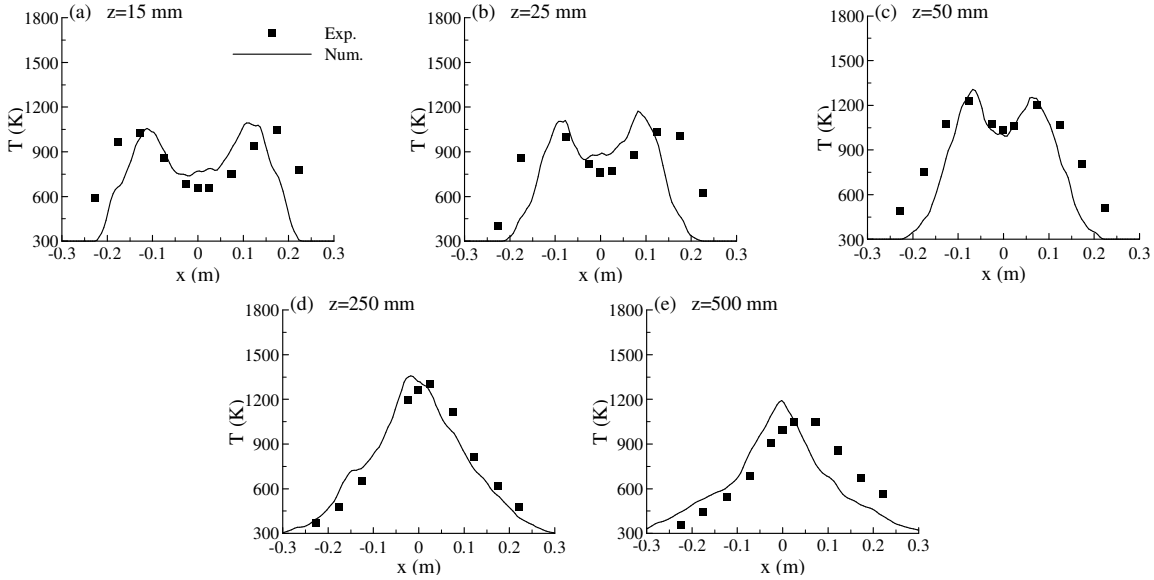

Figure 1. Radial profiles of temperature at different heights above the pool basis.

3.3. Temperature fluctuations

Figure 3 quantifies the turbulent intensity, defined as $\sqrt{\langle\widetilde{T''^2}\rangle}/\langle\tilde{T}\rangle$, as a function of the normalized height. In this figure the horizontal dashed line indicates the level 0.8 whereas the vertical dashed lines delimit the continuous flame (CF) and intermittent flame (IF) regions. The total temperature variance is computed as $\langle\widetilde{T''^2}\rangle = \langle\widetilde{T^2}\rangle - \langle\tilde{T}\rangle^2$ [36]. The turbulent intensity reaches a maximum value of the order of 0.5 in the IF region for the three flames.

This behaviour is in quantitative agreement with that reported from experiments on medium-scale methane pool fires by Cox and Chitty [37]. It should be pointed out that turbulent intensity for F4D reaches similar levels in both the CF and IF regions. Figure 3 shows also the ratio between the resolved temperature variance, $\langle \widetilde{T'^2} \rangle_{ReS} = \langle \tilde{T}^2 \rangle - \langle \tilde{T} \rangle^2$, and $\langle \widetilde{T'^2} \rangle$. It can be observed that more than 80% of temperature variance is on the whole resolved by the present LES for the three flames.

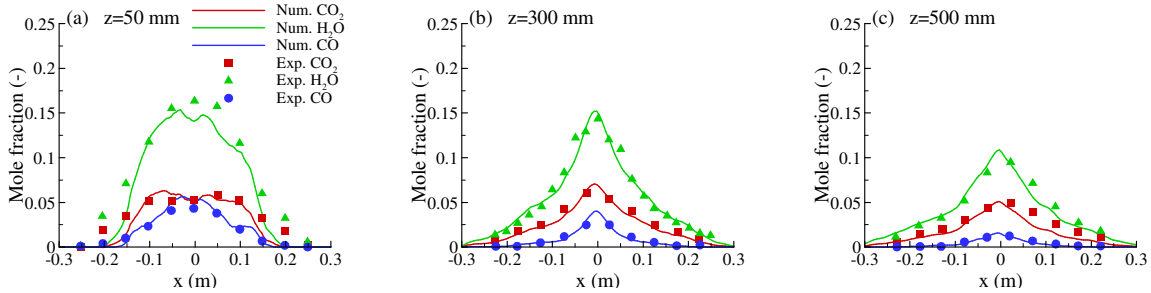

Figure 2. Radial profiles of mole fractions of CO, CO_2 and H_2O at different heights above the pool basis.

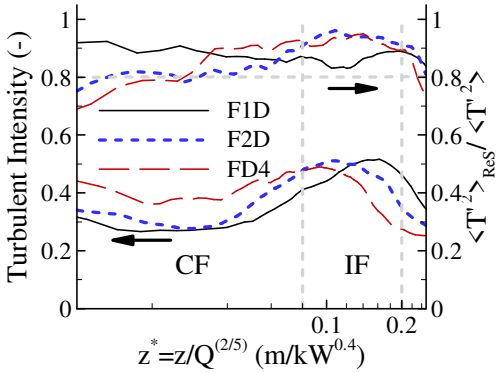

Figure 3. Centerline evolution of the turbulence intensity (left y-axis) and resolved-part of temperature variance (right y-axis) as a function the normalized height.

3.4. Effects of TRI on radiative loss

The radiant fraction can be re-expressed as $\chi_R = \chi_{em}\left(1 - \dot{Q}_{abs}/\dot{Q}_{em}\right)$. $\chi_{em} = \dot{Q}_{em}/\dot{Q}$ is the ratio of total emission to the HRR whereas $\dot{Q}_{abs}/\dot{Q}_{em}$ represents the part of total emission

reabsorbed within the flame, with $\left(1-\dot{Q}_{abs}/\dot{Q}_{em}\right)$ being the flame transparency [38]. χ_{em} increases significantly with the flame size from about 47% for F1D to more than 80% for F4D. On the other hand, $\dot{Q}_{abs}/\dot{Q}_{em}$ increases also with the flame size from 57% for F1D to 72% for F4D. Therefore, the moderate increase in χ_R with the flame size reported in Table 3 (Full TRI line) is explained by a balance between an enhancement in χ_{em} and a reduction of $\left(1-\dot{Q}_{abs}/\dot{Q}_{em}\right)$.

The contributions of the resolved-scale, SFS and total fluctuations to χ_R can be evaluated from the following decomposition:

$$(\chi_R)_{FullTRI} = (\chi_R)_{NoTRI} + \underbrace{\underbrace{[(\chi_R)_{ReSTRI} - (\chi_R)_{NoTRI}]}_{ReS\,TRI} + \underbrace{[(\chi_R)_{FullTRI} - (\chi_R)_{ReSTRI}]}_{SFS\,TRI}}_{TRI} \quad (7)$$

Table 3 shows that $(\chi_R)_{NoTRI}$ is around 0.04 for the three flames. This value is considerably lower than those of 0.19 measured by Fischer et al. [1] and 0.202 predicted by the Full TRI model for F1D (see Table 3). These differences highlight the importance of TRI in pool fires. The contribution of TRI to radiative loss is evaluated from $TRI = \frac{[(\chi_R)_{FullTRI}-(\chi_R)_{NoTRI}]}{(\chi_R)_{FullTRI}} \times 100$. Table 3 shows that TRI represents about 80% of the radiative loss. This high contribution agrees with the results reported in the literature for medium-scale non-luminous pool fires [7],[9] and can be explained, on the one hand, by the rather low time-averaged temperature in pool fires and, on the other hand, by the high level of turbulence intensity due to the puffing process (see Fig. 3). In addition, this percentage increases slightly with the flame size (see Table 3).

$ReS_{\chi_R} = \frac{[(\chi_R)_{ReS}-(\chi_R)_{NoTRI}]}{(\chi_R)_{FullTRI}} \times 100$ and $SGS_{\chi_R} = \frac{[(\chi_R)_{FullTRI}-(\chi_R)_{ReSTRI}]}{(\chi_R)_{FullTRI}} \times 100$ quantify the contributions of resolved and SFS fluctuations to χ_R, respectively (see Table 3). ReS_{χ_R} decreases as the pool size is enhanced from about 60% for F1D to 49% for F4D. On the other

hand, the contribution of SGS TRI to radiative loss appears to be significant and increases with the pool size. It represents about 18% for F1D and reaches 33% for F4D.

$SGS_{TRI} = \frac{[(\chi_R)_{FullTRI} - (\chi_R)_{ReSTRI}]}{[(\chi_R)_{FullTRI} - (\chi_R)_{NoTRI}]} \times 100$ quantifies the contribution of SFS fluctuation to TRI which increases from 23% for F1D to 40% for F4D. This illustrates further the increasing importance of the contribution of SGS TRI with the pool size.

Table 3. Effects of TRI closures on χ_R. The experimental value for F1D is 0.19 [1].

Flames	F1D	F2D	F4D
χ_R (-)			
Full TRI	0.202	0.215	0.244
ReS TRI	0.165	0.171	0.161
No TRI	0.043	0.040	0.041
Contribution of fluctuations to χ_R (%)			
TRI	78.94	81.35	83.33
ReS_{χ_R}	60.65	58.83	49.49
SGS_{χ_R}	18.29	22.52	33.83
Contribution of SFS to TRI			
SGS_{TRI}	23.17	27.68	40.6

3.5. Effects of SFS TRI on radiative heat flux

Figure 4 displays the axial distribution of the net radiative flux at a normalized distance of $r^* = r/\dot{Q}^{2/5}$ =0.18 m/kW$^{0.4}$ from the fire plume axis. This normalized distance corresponds to r =1m for F1D. Figure 4 shows that the net radiative flux increases on the whole with the pool size. Whatever the pool fire considered, the radiative flux is underestimated along the entire distribution when SFS TRI is disregarded and this underestimation becomes increasingly important as the pool size is enhanced. In particular, neglecting SFS TRI leads to an underestimation of the peaks of net radiative flux that by about 12.2%, 25.6% and 29.2% for F1D, F2D and F4D, respectively.

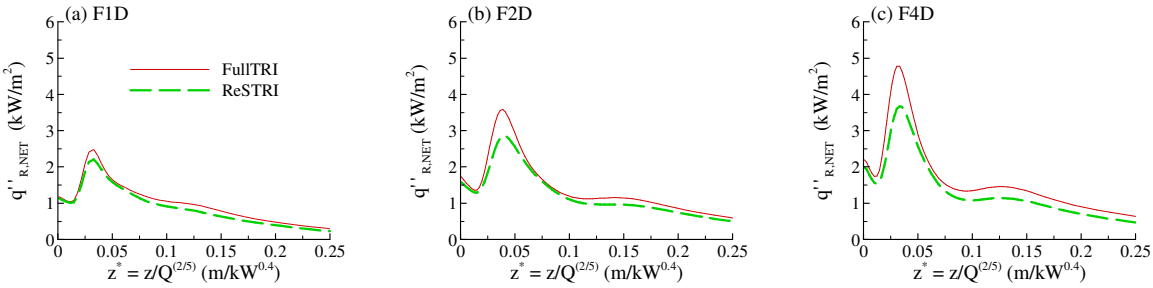

Figure 4. Effects of SFS TRI on the axial distribution of net radiative heat flux at a normalized distance of $r^* = r/\dot{Q}^{2/5}$ =0.18 m/kW$^{0.4}$ from the fire plume axis as a function of the normalized height.

3.6. Effects of SFS TRI on fire plume structure

Figures 5 and 6 display the temperature and the axial velocity along the fire plume axis. These figures show clearly that disregarding the SFS TRI affects the fire plume structures and the effects are enhanced with the pool size. For F1D, the radiative loss are underestimated by 18% when SFS TRI is not considered (see Table 3). As a results, the temperature is overpredicted in the IF region ($z^* > 0.08m/kW^{0.4}$) with a maximum deviation of 82K at $z^* = 0.2m/kW^{0.4}$ (see Fig. 5a). This induces an overestimation of the velocity by about 10% (see Fig. 6a). Figures 5a and 6a show that considering SFS TRI improves the predictions for F1D. For F2D, neglecting the SFS TRI leads to an underestimation of the radiative loss by about 22%. Figure 5b shows that the temperature peak is shifted downstream as compared to the Full TRI case and the maximum overestimation is 106 K at $z^* = 0.077m/kW^{0.4}$. The largest discrepancies are observed for F4D for which neglecting the SFS TRI leads to an overestimation of the temperature by about 200K along the entire plume axis and an overprediction of the axial velocity by about 19% at $z^* = 0.1m/kW^{0.4}$ (see Figs. 5c and 6c).

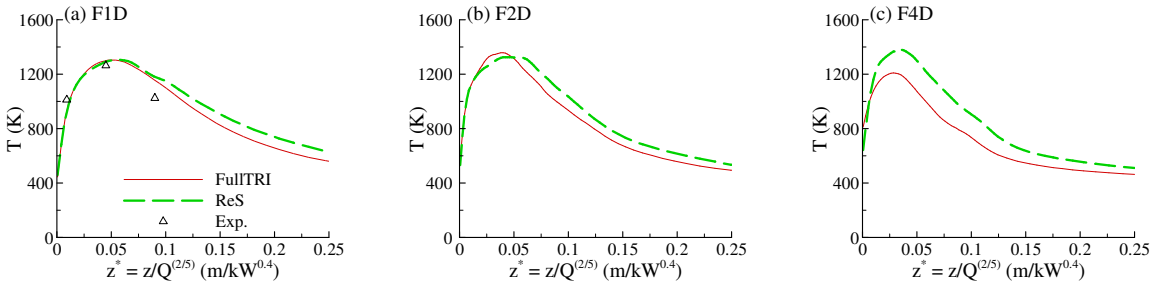

Figure 5. Effects of SFS TRI on the axial mean temperature as a function of the normalized height.

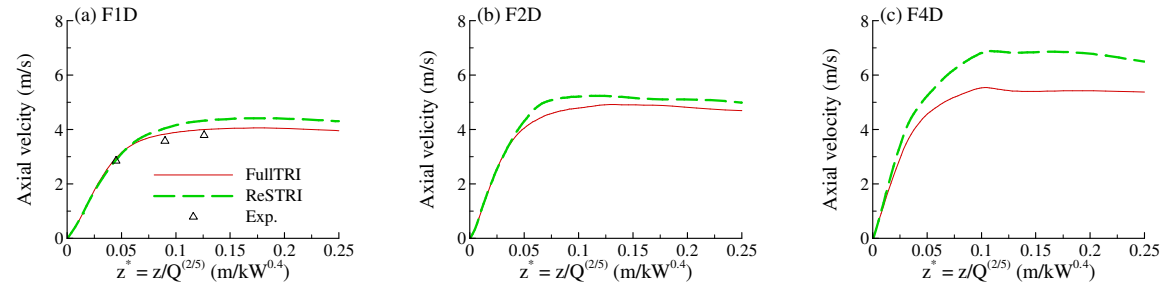

Figure 6. Effects of SFS TRI on the mean axial velocity as a function of the normalized height.

4. Conclusions

LES involving state of the art combustion and radiation sub-models have been exercised to evaluate and quantify the contributions of TRI in ethanol pool fires ranging from medium to large size. The following conclusions can be drawn:

1) The model reproduces well the experimental data in terms of temperature, species concentration, puffing frequency and radiant fraction.

2) TRI accounts for more than 80% of the radiative loss in non-luminous pool fires.

3) For LES that resolves more than 80% of the temperature variance, the contribution of SFS fluctuation to TRI increases with the pool size from 23% for a 0.5m diameter pool fire to more than 40% for a 2m diameter pool fire.

4) SFS TRI contributes for about 20% to radiative loss in the 0.5m diameter pool fire and this contribution increases with the pool size to reach about 33% for the 2m diameter pool fire. Its impact on the prediction of radiative heat flux and fire plume structure cannot be neglected even for medium-scale pool fires.

References

[1]. S.J. Fischer, B. Hardoin-Duparc, W.S. Grosshandler, The structure and radiation of an ethanol pool fire, Combust. Flame 70 (1987) 291-306.

[2]. M. Klassen, J.P. Gore, Temperature and soot volume fraction statistics in toluene-fired pool fires, Combust. Flame 93 (1993) 270-278.

[3]. A.Y. Snegirev, Statistical modeling of thermal radiation transfer in buoyant turbulent diffusion flames, Combust Flame 136 (2004) 51-71.

[4]. G.C. Fraga, P.J. Coelho, A.P. Petry, F.R.H. França, Development and testing of a model for turbulence-radiation interaction effects on the radiative emission, J. Quant. Spectros. Rad. Transf. 245 (2020) 106852.

[5]. G. Krishnamoorthy, A comparison of gray and non-gray modeling approaches to radiative transfer in pool fire simulations, J Hazard Mater 182 (2010) 570-80.

[6]. J.L. Consalvi, R. Demarco, A. Fuentes, S. Melis, J.P. Vantelon, On the modeling of radiative heat transfer in laboratory-scale pool fires, Fire Saf. J. 60 (2013) 73-81.

[7]. J.L. Consalvi, Influence of turbulence–radiation interactions in laboratory-scale methane pool fires, Int. J. Therm. Sci. 60 (2012) 122-130.

[8]. J.L. Consalvi, R. Demarco, A. Fuentes, Modelling thermal radiation in buoyant turbulent diffusion flames. Combust. Theory Model 16 (2013) 817-841.

[9]. G.C. Fraga, F.R. Centeno, A.P. Petry, P.J. Coelho, F.H.R. França, On the individual importance of temperature and concentration fluctuations in the turbulence-radiation interaction in pool fires, Int. J. Heat Mass Transf. 136 (2019) 1079–1089.

[10]. G.C. Fraga, P.J.Coelho, A.P.Petry, F.H.R. França, Investigation of the role of turbulent fluctuations on the time-averaged radiative emission in large-scale, turbulent pool fires, Fire Safety J. 112 (2020) 102945.

[11]. T.G. Ma, J.G. Quintiere, Numerical simulation of axi-symmetric fire plumes: accuracy and limitations, Fire Safety J. 38 (2003) 467–492.

[12]. Y. Xi, J.P. Gore, K.B. McGrattan, R.G. Rehm, H.R. Baum, Fire dynamics simulation of a turbulent buoyant flameusing a mixture-fraction-based combustion model, Combust. Flame 141 (2005) 329–335.

[13]. Y. Wang, P. Chatterjee, J.L. de Ris, Large eddy simulation of fire plumes, Proc. Combust. Inst. 33 (2011) 2473–2480.

[14]. P. Chatterjee, Y. Wang, K.V. Meredith, S.B. Dorofeev, Application of a subgrid soot-radiation model in the numerical simulation of a heptane pool fire, Proc. Combust. Inst. 35 (2015) 2573–2580.

[15]. G. Maragkos, T. Beji, B. Merci, Advances in modelling in CFD simulations of turbulent gaseous pool fires, Combust. Flame 181 (2017) 22–38.

[16]. G. Maragkos, T. Beji, B. Merci, Towards predictive simulations of gaseous pool fires, Proc. Combust. Inst. 37 (2019) 3927–3934.

[17]. I. Sikic, S. Dembele, J. Wen, Non-grey radiative heat transfer modelling in LES-CFD simulated methanol pool fires, J. Quant. Spectrosc. Radiat. Transf. 234 (2019) 78–89.

[18]. A. Gupta, D.C. Haworth, M.F. Modest, Turbulence-radiation interactions in large-eddy simulations of luminous and nonluminous nonpremixed flames, Proc. Combust. Inst. 34 (2013) 1281–1288.

[19]. J.L. Consalvi, F. Nmira, W. Kong, On the modeling of the filtered radiative transfer equation in large eddy simulations of lab-scale sooting turbulent diffusion flames, J. Quant. Spectrosc. Radiat. Transf. 221 (2018) 51–60.

[20]. F.C. Miranda, P.J. Coelho, F. di Mare, J. Janicka, Study of turbulence-radiation interactions in large-eddy simulation of scaled Sandia flame D, J. Quant. Spectrosc. Radiat. Transf. 228 (2019) 47–56.

[21]. A. Snegirev, E. Markus, E. Kuznetsov, J. Harris, Ted Wu, On soot and radiation modeling in buoyant turbulent diffusion flames, Heat Mass Transf. 54 (2018) 2275–2293.

[22]. L. Ma, F. Nmira, J.L. Consalvi, Verification and validation of a variable–density solver for fire safety applications, Numer. Heat Transf. B, 76 (2019) 107-129.

[23]. \Code Saturne." http://www.code-saturne.org.

[24]. P. Moin, K. Squires, W. Cabot, S. Lee, A dynamic subgrid-scale model for compressible turbulence and scalar transport, Phys. Fluids A 3 (1991) 2746-2757.

[25]. D. Carbonell, C.D. Perez-Segarra, P.J. Coelho, A. Oliva, Flamelet mathematical models for non-premixed laminar combustion, Combust. Flame 156 (2009) 334-347.

[26]. P. Saxena, F.A. Williams, Numerical and experimental studies of ethanol flames, Proc. Combust. Inst. 31 (2007) 1149-1156.

[27]. A.W. Vreman, B.A. Albrecht, J.A. van Oijen, L.P.H. de Goey, R.J.M. Bastiaans, Premixed and non-premixed generated manifolds in large-eddy simulation of Sandia flame D and F, Combust. Flame 153 (2008) 394-416.

[28]. C.M. Kaul, V. Raman, A posteriori analysis of numerical errors in subfilter scalar variance modeling for large eddy simulation, Phys. Fluids 23 (2011) 035102.

[29]. C. Jiménez, F. Ducros, B. Cuenot, B. Bédat, Subgrid scale variance and dissipation of a scalar field in large eddy simulations, Phys. Fluids 13 (2001) 1748-1754.

[30]. S.J. Fischer, W.L. Grosshandler, Radiance, soot, and temperature interactions in turbulent alcohol fires, Proc. Combust. Inst. 22 (1989) 12141-1249.

[31]. V.P. Solovjov, B.W. Webb, F. Andre, The rank correlated FSK model for prediction of gas radiation in non-uniform media, and its relationship to the rank correlated SLW model, J. Quant. Spectrosc. Radiat. Transf. 214 (2018) 120-132.

[32]. M.F. Modest, R.J. Riazzi, Assembly full spectrum k-distribution from a narrow band database: effects of mixing gases, gases and non-gray absorpting particles and non-gray scatters in non-gray enclosures, J. Quant. Spectrosc. Radiat. Trans. 90 (2005) 169-189.

[33]. L.S. Rothman, I.E. Gordon, R.J. Barber, H. Dothe, R.R. Gamache, A. Goldman, V.I. Perevalov, S.A. Tashkun, J. Tennyson, HITEMP: the high-temperature molecular spectroscopic database, J. Quant. Spectrosc. Radiat. Transfer 111 (2010) 2139-2150.

[34]. M.F. Modest, Radiative Heat Transfer, Third ed., Academic Press, New York, 2013.

[35]. K.A. Jensen, J.F. Ripoll, A.A. Wray, D. Joseph, M. El Hafi, On various modeling approaches to radiative heat transfer in pool fires, Combust. Flame 148 (2007) 263–279.

[36]. D. Veynante, R. Knikker, Comparison between LES results and experimental data in reacting flows, J. Turbulence 7 (2006) 2006.

[37]. G. Cox, R. Chitty, Some stochastic properties of fire plumes, Fire Materials 6 (1982) 127-134.

[38]. J.L. Consalvi, F. Nmira, Modeling of large-scale under-expanded hydrogen jet fires, Proc. Combust. Inst. 37 (2019) 3943-3950.

List of figure captions

Figure 1. Radial profiles of temperature at different heights above the pool basis.

Figure 2. Radial profiles of mole fractions of CO, CO_2 and H_2O at different heights above the pool basis.

Figure 3. Centerline evolution of the turbulence intensity (left y-axis) and resolved-part of temperature variance (right y-axis) as a function the normalized height.

Figure 4. Effects of SFS TRI on the axial net heat flux at a normalized distance of $r^* = r/\dot{Q}^{2/5}$ =0.18 m/kW$^{0.4}$ from the fire plume axis as a function of the normalized height.

Figure 5. Effects of SFS TRI on the axial mean temperature as a function of the normalized height.

Figure 6. Effects of SFS TRI on the mean axial velocity as a function of the normalized height.